Inorganic Chemistry

Article

pubs.acs.org/IC

Computational Mechanistic Study of the Hydrogenation of Carbonate to Methanol Catalyzed by the Ru^{II}PNN Complex

Haixia Li, Mingwei Wen, and Zhi-Xiang Wang*

College of Chemistry and Chemical Engineering, Graduate University of the Chinese Academy of Sciences, Beijing 100049, China

Supporting Information

ABSTRACT: Density functional theory computations have been carried out to study the mechanism of hydrogenation-based transformation of dimethyl carbonate to methanol, catalyzed by Ru^{II}PNN catalyst. The energetic results show that the catalytic transformation includes three sequential stages consistently involving the catalyst: (stage I) transformation of dimethyl carbonate (**3**) to methyl formate (**5**) and methanol; (stage II) transformation of methyl formate **5** to formaldehyde and methanol; (stage III) hydrogenation of formaldehyde to methanol. Stages I and II proceed similarly and follow three steps: hydrogen activation, formation of a hemiacetal intermediate via stepwise hydrogen transfer to dimethyl carbonate in stage I or methyl fomate in stage II, and subsequent decomposition of the hemiacetal intermediate to afford methanol. Hydrogenation via carbonyl insertion into the Ru−H bond is less favorable than the stepwise hydrogen-transfer mechanism. Decomposition of hemiacetal takes places by first breaking the hemiacetal O−H bond to give an alkoxide complex, followed by deprotonation of the benzylic arm ligand to the adjacent methoxy group. Comparing the hydrogenation steps in the three stages, hydrogenation in stage I is most difficult, that in stage II is less difficult, and that in stage III is easiest in terms of both kinetics and thermodynamics. This can be ascribed to the stronger electrophilicity of the carbonyl group in methyl formate or formaldehyde than that in dimethyl carbonate and fewer steric effects between the catalyst and methyl formate or formaldehyde than that between the catalyst and dimethyl carbonate. Thermodynamically, both stages I and II are uphill, but stage III is downhill significantly, which is the driving force for the catalytic transformation. The study indicates that the methanol product could facilitate the hydrogen activation involved in the transformation, implying that transformation could be accelerated by initially adding methanol.

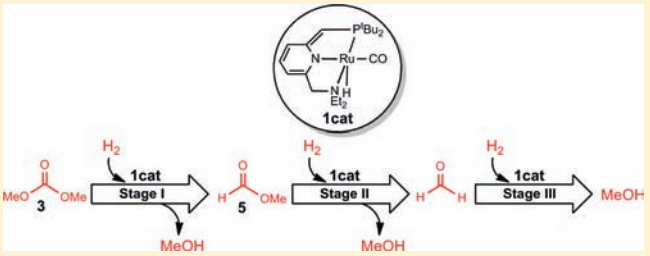

1. INTRODUCTION

Hydrogenation is an effective and environmentally benign approach to perform chemical transformations using H_2 as the feedstock. Much effort made in the past 4 decades has allowed hydrogenation to conveniently transform ketones and imines to alcohols and amines, respectively.[1−3] Yet, homogeneous hydrogenations of esters[4] and amides[5] were rarely reported. Because the carbonyl groups in esters and amides have lower electrophilicity caused by resonance effects involving alkoxy or amino groups, it is more difficult to hydrogenate esters and amides than ketones and imines. The difficulty to hydrogenate esters can be perceived from the fact that hydrogenation of ester [MeC(O)OMe] is 6.2 kcal/mol less exergonic than hydrogenation of ketone (Me_2C=O).[6a] Previously, hydrogenation of methyl formate could only be performed heterogeneously under high pressure and temperature.[7] Nonetheless, Milstein and co-workers recently demonstrated that their pincer Ru^{II}PNN complexes (i.e., **1cat** and **2cat** in Scheme 1) were able to hydrogenate esters and amides, giving alcohols (eq 1) and a mixture of alcohols and amines (eq 2), respectively.[4b,5b] Most recently, the group further showed that the catalysts **1cat** and **2cat** could perform hydrogenations of carbonate **3** (eq 3) and carbamate **4** (eq 4).[8] The unprecedented catalytic hydrogenations of urea derivatives to amines and methanol have been realized by using **2cat**.[9] Because of the enhanced resonance effect due to two alkoxy groups in carbonates or one alkoxy and one amino group in carbamates, hydrogenations of carbonates and carbamates are even more challenging. Because hydrogenations of ketones and imines are exergonic, hydrogenations of carbonates are endergonic; hydrogenation of MeOC(O)OMe to give MeOCH(OH)OMe is endergonic by 11.3[2.5] kcal/mol ($\Delta G[\Delta H]$).[6b] Furthermore, organic carbonates can even be used as solvents in homogeneous catalytic hydrogenations.[10]

The study of hydrogenations of carbonates and carbamates is not only of fundamental importance in pushing the envelope of catalytic hydrogenation but also of practical use. Such hydrogenation reactions may provide an indirect route to transforming CO_2 into methanol if conversion of CO_2 into carbonates and carbamates can be realized efficiently and economically. The advance in conversion of CO_2 into carbonates and carbamates has been reviewed by Sakakura et al.[11]

Received: January 24, 2012
Published: May 8, 2012

dx.doi.org/10.1021/ic300175b | Inorg. Chem. 2012, 51, 5716−5727

Scheme 1. Schematic Drawings of 1cat and 2cat and Hydrogenations of Ester (eq 1), Amide (eq 2), Dimethyl Carbonate (3; eq 3), and Methyl Carbamate (4; eq 4)

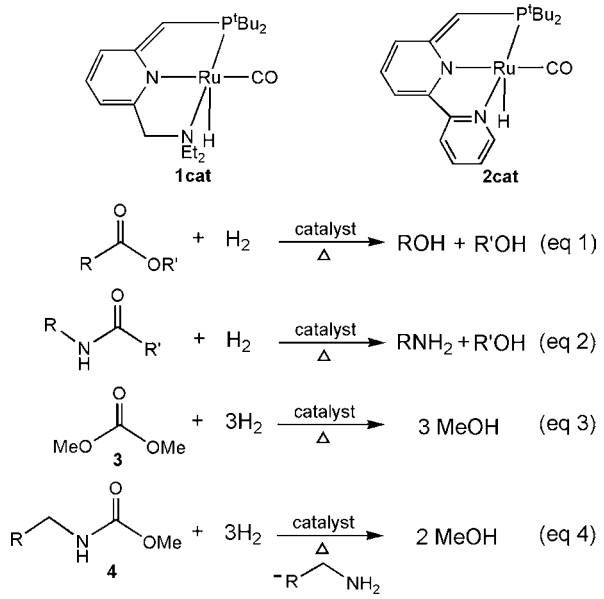

The pincer catalysts such as **1cat** and **2cat** exhibit high catalytic activity involving σ-bond activations (e.g., H−H, C−H, N−H, and O−H bond activations).[12,13] The catalytic power of such pincer complexes in activating the σ bond originates from their novel electronic structures, including the bifunctional active sites composed of sp^2C of the =CHP^{t}Bu$_2$ arm (sp^2C represents the carbon atom of the =CHP^{t}Bu$_2$ arm herein and hereafter) and the metal centers and aromatization effect enabled through the six-membered ring ligand, which is nonaromatic in the catalyst but becomes an aromatic pyridine ring in the σ-bond activation product.[14,15] The σ-bond activation can be considered as a formal [2 + 2 + 2] addition involving the two π electrons of the C=C bond, the two lone-pair electrons of the nitrogen atom, and the two σ electrons of the σ bond (Scheme 2A). The aromaticity due to the involvement of six electrons stabilizes the activation transition states and thus lowers the activation barriers. By mimicking these characteristics of the pincer complexes (Scheme 2B), we computationally designed several metal-free counterparts that can activate hydrogen reversibly on the basis of the computed energies.[16] The catalytic roles of such pincer complexes in mediating some novel reactions have been investigated by several groups.[13,14] Recently, we computationally studied the catalytic mechanism of **1cat**-catalyzed amide formation from alcohols and amines.[17] In this study, we focus on the catalytic mechanism for hydrogenation of carbonates to give methanol.

Scheme 2. (A) Schematic Elucidation of 1cat-Mediated Hydrogen σ-Bond Activation via [2 + 2 + 2] Addition and (B) Schematic Illustration of the Design of Metal-Free Counterparts of 1cat[a]

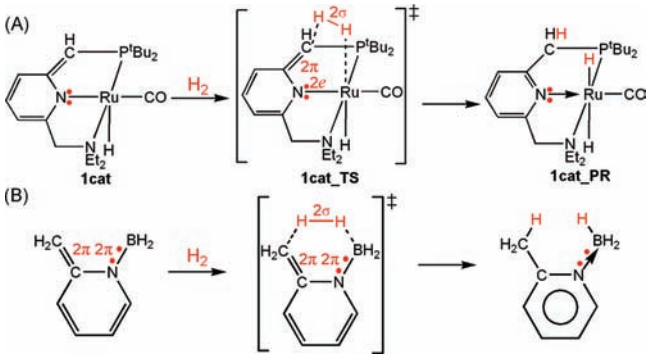

[a]Note that the molecule in part B is just a model (see ref 16 for details).

2. COMPUTATIONAL DETAILS

All of the structures were optimized and characterized as minima or transition states at the TPSSTPSS[18]/BSI level [BSI designates the basis set combination of LANL2DZ[19] for the ruthenium atom and 6-31G (d,p) for all nonmetal atoms]. The choice of TPSSTPSS was based on Hall and co-workers' success in applying the method to study the light-induced water-splitting reaction catalyzed by **1cat**.[15b] When necessary, intrinsic coordinate reaction (IRC) calculations were carried out to examine the connection of a transition state with its backward and forward minima. At the TPSSTPSS/BSI structures, the energetic results were further refined by single-point calculations at the M06[20]/BSII level with solvation effects accounted for by the SMD[21] solvent model using the experimentally used 1,4-dioxane solvent, where BSII denotes the basis set combination of SDD[22] for the ruthenium atom and 6-31++G(d,p) for all nonmetal atoms.

The gas-phase TPSSTPSS/BSI harmonic frequencies were used for the thermal and entropic corrections to the enthalpies and free energies at 298.15 K and 1 atm. It should be noted that the ideal gas-phase model intrinsically overestimates the entropic contributions because of ignoring the suppressing effect of the solvent on the rotational and transitional freedoms of the substrates.[23−26] Accurate prediction of the entropies in solution is still a challenge for computational chemistry, and no standard approach is currently available. Nevertheless, Martin, Hay, and Pratt (MHP)[26] have proposed a scheme to correct the overestimation of entropic contributions, that is, artificially raising the pressure from 1 to 1354 atm (termed the MHP scheme hereafter). According to the approach, an additional 4.3 kcal/mol free-energy correction applies to each component change for a reaction at 298.15 K and 1 atm [i.e., a reaction from m to n components has an additional free-energy correction of $(n - m) \times 4.3$ kcal/mol]. Experimentally, Yu and co-workers[24] have demonstrated that the ideal gas-phase model overestimated entropic contributions by 50−60% in their addition reactions. On the basis of the experimental results, we applied a scaling factor of 0.5 to the gas-phase entropic contributions (i.e., $-T\Delta S$) as a rough estimate (termed the Yu scheme hereafter). The uncorrected M06 (SMD, 1,4-dioxane)/BSII//TPSSTPSS/BSI free energies (i.e., enthalpies in the solvent plus $-T\Delta S$ value in the gas phase) are used in the discussion of the mechanistic details, aided by the free energies corrected by the MHP and Yu schemes when necessary. It should be noted that applications of both correction schemes do not change our predicted mechanism. Meanwhile, we give the enthalpy results in the schemes and figures for reference.

To ascertain the mechanism drawn from M06 (SMD)/BSII/TPSSTPSS/BSI computations, we employed M06 and ωB97X-D[27] density functional theory (DFT) functionals and larger basis sets to recalculate the key stationary points selected on the basis of M06 (SMD)/BSII/TPSSTPSS/BSI energy profiles.

dx.doi.org/10.1021/ic300175b | Inorg. Chem. 2012, 51, 5716−5727

Scheme 3. (A) Mechanism for Hydrogenation of Dimethyl Carbonate 3 to Methanol Proposed by Milstein and Co-workers and (B) Mechanism Revealed by the Present Study

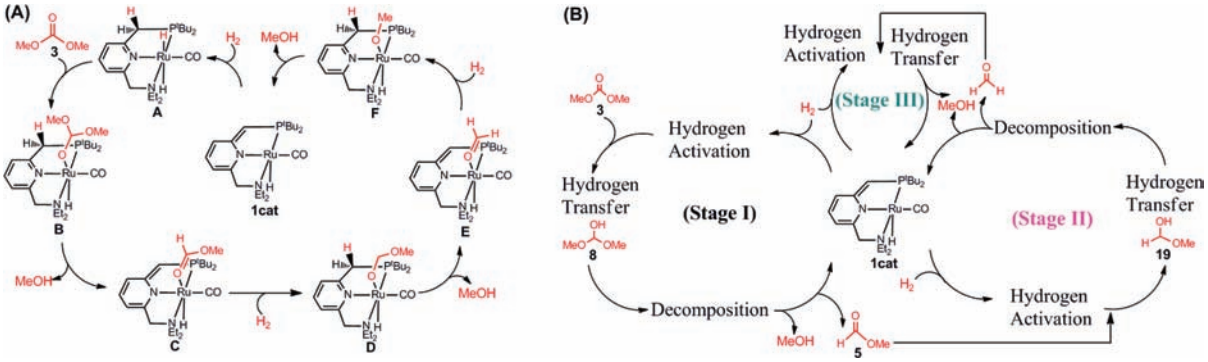

These were optimized and characterized as minima or transition states at the M06/BSIII and ωB97X-D/BSIII levels (BSIII designates the basis set combination of SDD for the ruthenium atom and 6-31G (d,p) for all nonmetal atoms), respectively. Using M06/BSIII and ωB97X-D/BSIII-optimized structures, the energetic results were further refined by single-point calculations at the respective M06/BSIV and ωB97X-D/BSIV levels with solvation effects accounted for by the SMD solvent model, where BSIV denotes the basis set combination of def2-TZVPP[28] for the ruthenium atom and 6-311++G(d,p) for all nonmetal atoms. The gas-phase M06/BSIII and ωB97X-D/BSIII harmonic frequencies were used for the thermal and entropic corrections to the enthalpies and free energies at 298.15 K and 1 atm. All calculations were carried out by using *Gaussian 03*[29] and *Gaussian 09*[30] programs.

3. RESULTS AND DISCUSSION

Milstein and co-workers have shown that the catalysts **1cat** and **2cat** can efficiently hydrogenate both carbonates (e.g., dimethyl carbonate **3**) and carbamates (e.g., **4**) to produce methanol (eq 3 and eq 4 in Scheme 1) and the bipyridine-based catalyst **2cat** performed better than **1cat**.[8] On the basis of their more elaborated experimental study of the **1cat**-catalyzed eq 3 reaction, they postulated a mechanism for the complete transformation of **3** into three methanol molecules (Scheme 3A). Hydrogen first adds to the bifunctional active site of the catalyst **1cat** constructed by sp^2C and ruthenium centers, leading to the *trans*-dihydride complex **A**. Subsequent hydride transfer to the carbonyl group of carbonate **3** gives the intermediate **B**. This step was proposed to take place via direct hydride attack on the carbonyl group or alternatively via dissociation of the $-CH_2NEt_2$ arm to provide a site for dimethyl carbonate coordination. Deprotonation of the $-CH_2P^tBu_2$ arm of **B** by the adjacent methoxyl group then results in liberation of methanol and formation of a dearomatized intermediate **C**, which bears coordinated methyl formate. The production of the second methanol takes place via dihydrogen addition to **C**, leading to an intermediate **D**. This process was proposed to proceed via the $-CH_2NEt_2$ arm opening, followed by hydride transfer to methyl formate. Deprotonation of the $-CH_2P^tBu_2$ arm of **D** by the methoxyl group delivers the second methanol molecule and **E**. The step from **E** to **F** proceeds through a mechanism similar to that from **C** to **D**. Methanol liberation from **F** regenerates catalyst **1cat**, completing the catalytic cycle.

We also selected the eq 3 reaction without any simplification for our mechanistic investigation. As sketched by Scheme 3B, the present study shows that the whole transformation takes places via three sequential stages with persistent participation of **1cat**: (stage I) H_2 + **3** (dimethyl carbonate) → methanol + **5** (methyl formate); (stage II) **5** + H_2 → methanol + formaldehyde; (stage III) H_2 + formaldehyde → methanol. The first two stages follow a similar mechanism including three steps: hydrogen activation, hydrogen transfer leading to hemiacetal intermediate, and decomposition of the hemiacetal intermediate to give methanol and the carbonyl compound (i.e., methyl formate **5** in stage I or formaldehyde in stage II). The third stage is a conventional hydrogenation. In the following, we will discuss the transformation in terms of the three stages and meanwhile compare our predicted mechanisms with other alternatives including those postulated previously.

3.1. Transformation of Dimethyl Carbonate to Methyl Formate and Methanol (Stage I). Our computed mechanism for releasing the first methanol molecule (stage I) is shown in Figure 1A, along with the free-energy profile (Figure 1B). The optimized structures of the key stationary points labeled in Figure 1 are displayed in Figure 2. The stage can be divided into three steps: hydrogen activation from **1cat** + H_2 to **6**, double hydrogen transfer to give a hemiacetal intermediate (**8**) from **6** + **3** to **8** + **1cat**, and decomposition of the hemiacetal intermediate to give methanol and methyl formate from **8** + **1cat** to MeOH + **5** + **1cat**. We discuss below stage I in terms of the three steps.

Hydrogen Activation To Give the trans-Dihydride Complex ***6****.* Similar to any catalytic hydrogenation, molecular hydrogen first needs to be activated by catalysts.[1−3,31,32] Hydrogen activation by catalyst **1cat** is heterolytic and produces the *trans*-dihydride complex **6** with a protonic hydrogen added to sp^2C of the $=CHP^tBu_2$ arm and a hydridic hydrogen to the ruthenium center. The activation barrier (25.6 kcal/mol, **TS1**) and small exergonicity (2.2 kcal/mol) signify that activation is nearly reversible, meeting the requirement for catalytic hydrogenation. Prior to **TS1**, a dihydrogen coordination complex (not shown in Figure 1) could be located, but it is 6.6 kcal/mol less stable than **1cat** + H_2. The six-membered-ring ligand in **1cat** is nonaromatic and exhibits a bond-length alternation consistent with its Lewis structure description. After hydrogen activation, the six-membered ring in **6** becomes an aromatic pyridine ring with nearly equal C−C bond lengths (ca. 1.400 Å). The aromatization effect enabled through the six-membered-ring ligand benefits hydrogen activation, which allows the weaker Lewis basic sp^2C center to be a Lewis base partner to construct a bifunctional active site with ruthenium to activate hydrogen. In comparison, the conventional metal−

dx.doi.org/10.1021/ic300175b | *Inorg. Chem.* 2012, 51, 5716−5727

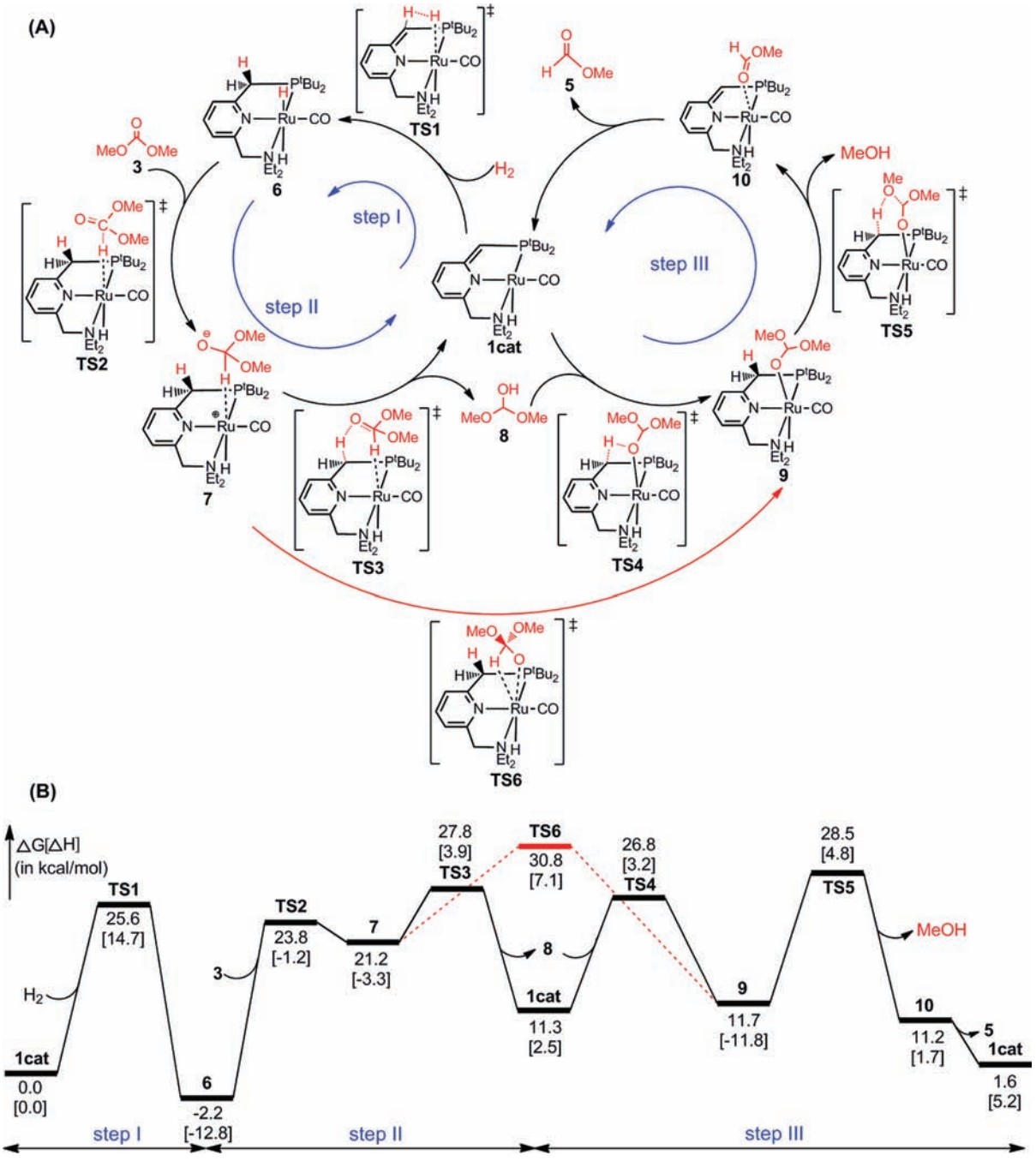

Figure 1. (A) Catalytic mechanism for hydrogenation of carbonate (**3**) to methyl formate **5** and methanol and (B) free-energy profile corresponding to part A. The IRC results for verification of the pathway are detailed in SI1 in the Supporting Information.

ligand bifunctional hydrogenation catalysts often use metal−X (X = N, O, and S) linkages as bifunctional active sites that contain stronger Lewis base partners (i.e., N, O, and S).[3,31,33]

The transformation produces methanol as the finial product. Whether methanol can facilitate hydrogen activation was examined. In the first scenario, as illustrated by the transition state **TS7** in Figure 3, methanol acts as a bridge, transferring its hydroxyl hydrogen to the sp^2C center and simultaneously obtaining a hydrogen atom by breaking dihydrogen through cooperation with the Lewis acidic Ru^{II} center. The optimized structure of **TS7** confirms the activation mode. Because the oxygen atom is more Lewis basic than sp^2C of the $=CHP^tBu_2$ arm, the enthalpy barrier (4.7 kcal/mol) of **TS7** is substantially lower than the 14.7 kcal/mol of **TS1**. Consistently, the dihydrogen bond length (0.861 Å) in **TS7** is shorter than 1.029 Å in **TS1**. However, the methanol-aided hydrogen activation by **1cat** involves three components, which results in a larger entropic penalty than the bimolecular activation (**TS1**). In terms of free energy, **TS7** is 1.3 kcal/mol higher than **TS1**. Considering that the free-energy correction (22.2 kcal/mol) was overestimated by the ideal gas-phase model, we speculate that hydrogen activation can be facilitated by the methanol product as the reaction proceeds. After MHP and Yu correction schemes are applied to the entropic contributions ($-T\Delta S$) to the free energies, **TS7** is 3.0 and 4.3 kcal/mol lower than **TS1**, respectively. Because the speculation needs experimental

dx.doi.org/10.1021/ic300175b | Inorg. Chem. 2012, 51, 5716−5727

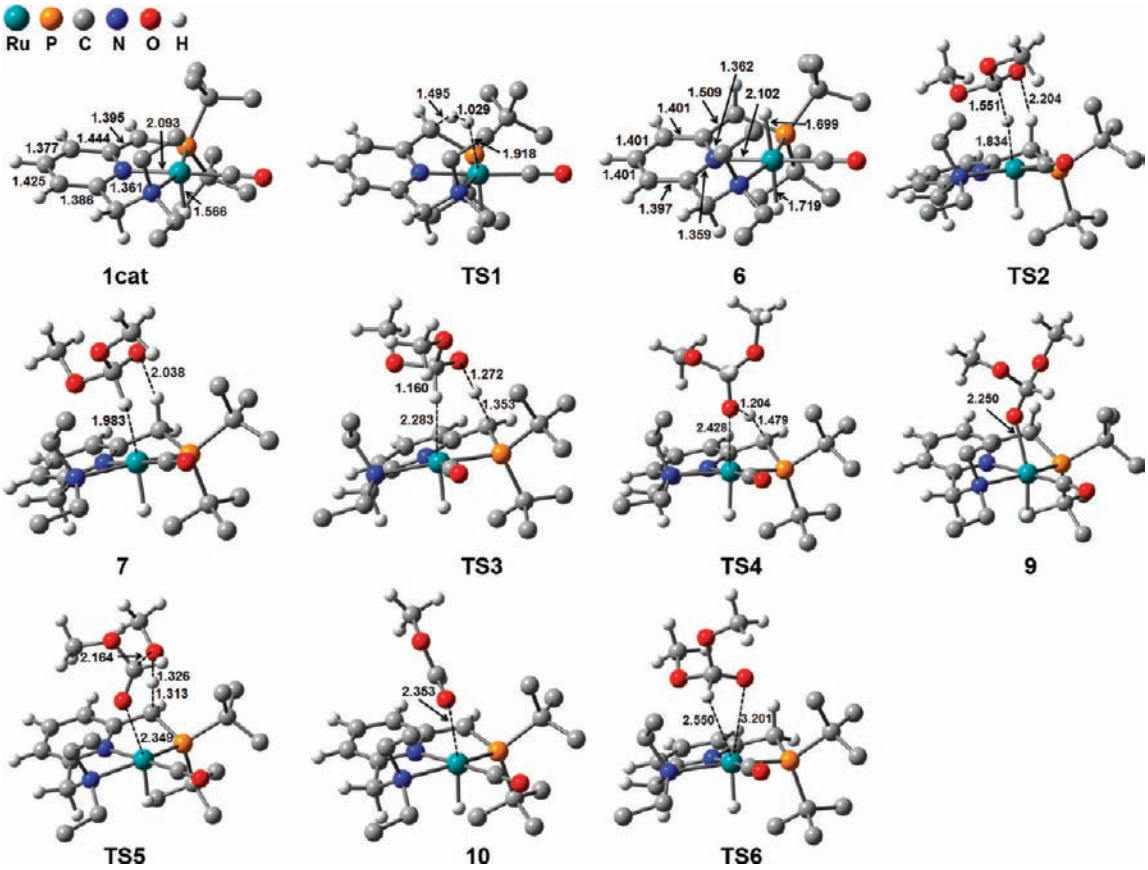

Figure 2. Optimized geometries of the key stationary points shown in Figure 1, along with the key bond lengths in angstroms. Trivial hydrogen atoms are omitted for clarity.

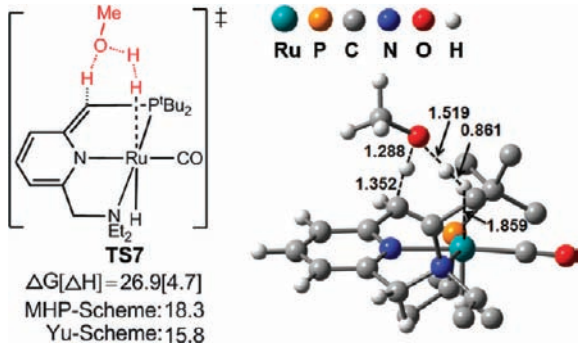

Figure 3. Optimized geometry of the transition state for methanol-aided hydrogen activation by **1cat**, along with the key bond lengths in angstroms. The barriers in kilocalories per mole are relative to **1cat** + H_2 + methanol. Trivial hydrogen atoms are omitted for clarity.

verification, there have been experiments to show that alcohol could facilitate hydrogen activation.[34,35] If this is true, the transformation may be improved by initially adding methanol.

The second scenario considered for methanol-assisted hydrogen activation was based on a recent study of Yang, who reported an EtOH-assisted hydrogen activation mechanism that can compete with direct hydrogen activation in the ketone hydrogenation catalyzed by an iron pincer complex (PNP)FeH(CO)Br, where PNP = 2,6-bis-(diisopropylphosphinomethyl)pyridine.[36] A similar mechanism is illustrated in Figure 4. Methanol first adds to the catalyst **1cat** by breaking its O−H bond, generating the complex **12**. The barrier (**TS8**) is 18.6 kcal/mol relative to **1cat** + MeOH, and the process is endergonic by 6.5 kcal/mol. Dissociation of the MeO^- group from **12** to give **13** + MeO^- further raises the energy of the system to 58.7 kcal/mol measured from methanol + **1cat**, implying that such a hydrogen activation mechanism could not occur in the present system. The transition state (i.e., the assumed **TS9**) for the following hydrogen activation could not be located. The solvent effect could be one of the factors responsible for the difference. The iron-complex-catalyzed ketone hydrogenation was conducted in a polar solvent (ethanol; ε = 24.9), while the present reaction was performed in 1,4-dioxane (ε = 2.2). If ethanol is applied as a solvent in the current reaction, the formation of the cationic complex **13** plus MeO^- is only endergonic by 9.6 kcal/mol, which is much less than the value (58.7 kcal/mol) in 1,4-dioxane. Because dissociation of the MeO^- group from **12** to give the cationic species **13** is a very high energy demand process, we did not further pursue the pathway.

Hydrogen Transfer. Hydrogen activation results in the *trans*-dihydride complex **6**. The next step is hydrogen transfer, transferring the activated hydrogen atoms to the carbonyl group of dimethyl carbonate **3**. This step is the reverse process of alcohol dehydrogenation. Our previous study on the alcohol dehydrogenation catalyzed by **1cat** showed that the double-hydrogen-transfer mechanism is more favorable than the β-hydrogen-elimination mechanism.[17] The double-hydrogen-transfer pathway (i.e., **6** + **3** → **TS2** → **7** → **TS3** → **1cat** + **8** in Figure 1) was again found to be more favorable than the alternative pathway via carbonyl insertion into the Ru−H bond, which will be discussed later. The optimized structures of the transition states (**TS2** and **TS3** in Figure 2) indicate that

dx.doi.org/10.1021/ic300175b | *Inorg. Chem.* 2012, 51, 5716−5727

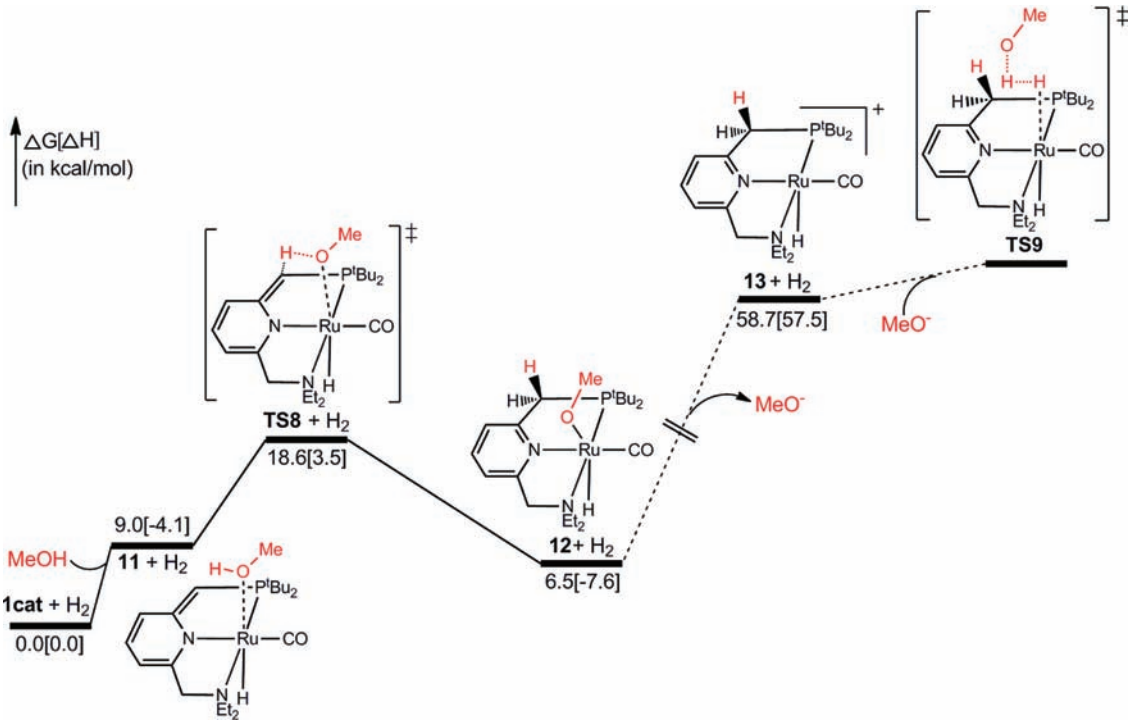

Figure 4. Catalytic mechanism for hydrogen activation via the first addition of methanol to **1cat**, together with the relative free energies and enthalpies. The optimized structures of the stationary points are given in SI2 in the Supporting Information.

hydrogen transfer takes place sequentially. The hydridic hydrogen on the Ru^{II} center first transfers to the carbonyl carbon atom of **3**, leading to an intermediate **7**, and the protonic hydrogen of the $-CH_2P^tBu_2$ arm of **7** then moves to the carbonyl oxygen atom. The free energies of **TS2** and **TS3** relative to **1cat** + **3** + H_2 are 23.8 and 27.8 kcal/mol, respectively. Hydrogen addition to **3** giving **8** + **1cat** is endergonic by 11.3 kcal/mol, which is in contrast to the general exergonic ketone hydrogenation, indicating that hydrogenation of carbonates is thermodynamically more difficult than ketone hydrogenation.

*Decomposition of Hemiacetal **8** to Methyl Formate **5** and Methanol.* Under catalysis of **1cat**, the formed hemiacetal intermediate **8** (the hydrogenation product of **3**) can be decomposed into more stable methyl formate with the release of one methanol molecule through the pathway **1cat** + **8** → **TS4** → **9** → **TS5** → **10** → **1cat** + **5** + MeOH. Decomposition starts by using **1cat** to break the O−H σ bond of the hemiacetal **8** via the transition state **TS4**. The barrier (**TS4**) for the O−H bond breaking is 15.5 kcal/mol relative to **8**, indicating that the process occurs facilely. Note that, prior to **TS4**, there is a complex between **8** and **1cat** (not shown in Figure 1) that is 12.2 kcal/mol higher than **8** + **1cat**. The intermediate complex **9** is 0.4 kcal/mol higher than **1cat** + **8**. When **9** is formed, the methoxy group abstracts the protonic hydrogen of the $-CH_2P^tBu_2$ arm of **9** to give **10** with the concurrent release of the first methanol via transition state **TS5**. The long C−O distance (2.164 Å) and the short O−H bond length (1.326 Å) in **TS5** (Figure 2) confirm the C−O bond-breaking and O−H bond-forming processes. The products (**10** + methanol) are 11.2 kcal/mol less stable than the energy reference (**1cat** + H_2 + **3**). However, a favorable entropic driving force can promote the release of **5** from complex **10**; the formation of **5** + **1cat** from **10** lowers the system down by 9.6 kcal/mol. Note that, after the MHP and Yu schemes are applied, 5 + **1cat** is still 5.3 and 3.0 kcal/mol more favorable than **10**. Overall, the transformation of **3** + H_2 to methyl formate **5** plus methanol is slightly endergonic by 1.6 kcal/mol. Referring to Figure 1, because hydrogenation of **3** to give **8** (steps I and II) is thermodynamically unfavorable, it would be difficult if there is no further driving force. However, the decomposition step (from **8** + **1cat** to MeOH + **5** + **1cat**) is downhill by 9.7 kcal/mol, providing a driving force for the thermodynamically unfavorable hydrogenation from **3** + **6** to **8**. The released methyl formate **5** could be further hydrogenated, which will be discussed in the next section.

Other Possible Pathways. As an alternative to the pathway **7** → **TS3** → **1cat** + **8** → **TS4** → **9** involving formation of the hemiacetal **8**, the intermediate **7** could pass a transition state (**TS6**) to reach **9** directly. The transition state **TS6** is higher than **TS3**/**TS4** in terms of either the enthalpy (3.2/3.9 kcal/mol) or free energy (3.0/4.0 kcal/mol), respectively, implying that the pathway is less favorable. This is reasonable because the transition state **TS6** breaks the favorable Ru···H−C[37] and H···O═C hydrogen-bonding interactions between the two moieties. To verify this, we further compared the energetic results of the two corresponding processes (**TS2** → **7** → **TS3** → **8** + **1cat** → **TS4** → **9** and **7** → **TS6** → **9**) involved in the alcohol dehydrogenation substep in amide formation via the coupling of alcohol and amine.[17] Previously, we did not find the transition state corresponding to **TS6**. In this study, we relocated the corresponding transition state. As detailed in SI3 in the Supporting Information, at the current level, the **TS6** counterpart was predicted to be 10.4 kcal/mol higher than the highest among the counterparts of **TS2**, **TS3**, and **TS4**. The comparisons further verify that the double-hydrogen-transfer pathway is more favorable than the direct pathway (**7** → **TS6** → **9**). As can be seen in the next section, a similar pathway is also less favorable in the second stage of hydrogenation of methyl formate **5**.

dx.doi.org/10.1021/ic300175b | *Inorg. Chem.* 2012, 51, 5716−5727

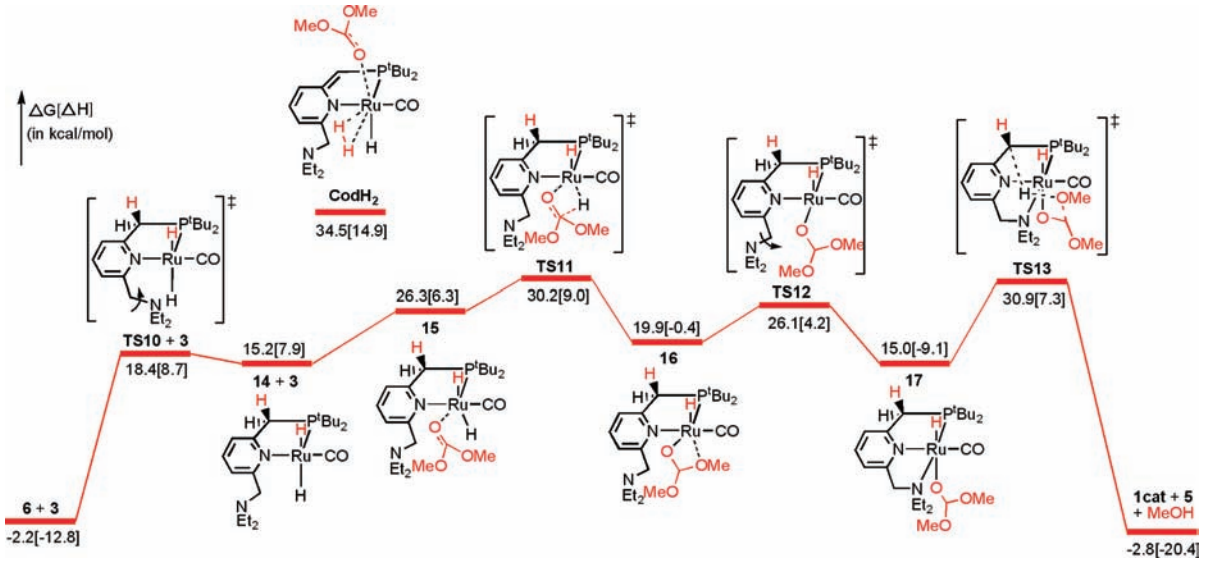

Figure 5. Free-energy profile for hydrogenation of the carbonate **3** to methyl formate **5** and methanol via carbonyl insertion into the Ru−H bond mechanism. Free energies and enthalpies in brackets are relative to **1cat** + **3** + H_2. Optimized geometries of the stationary points are given in SI5 in the Supporting Information. The IRC results for verification of the mechanism are detailed in SI1 in the Supporting Information.

The complex **7** also could dissociate to the anionic $(MeO)_2CHO^-$ and cationic complex **13**, which then reassociate to form the complex **9**. Because the dissociation products $[(MeO)_2CHO^-$ + **13**] are 29.4 kcal/mol higher than the complex **7** and much higher than **TS3**, **TS4**, and **TS6**, this pathway can be safely excluded.

As shown in Scheme 3A, it was postulated that the structure **A** (i.e., **6** in Figure 1A) could reach **B** (i.e., **9**) directly via insertion of the C═O bond of **3** into the Ru−H bond of **6** with or without opening the $-CH_2NEt_2$ arm.[8] We first considered the scenario via opening the $-CH_2NEt_2$ arm. This pathway was also proposed in ester hydrogenation catalyzed by a similar catalyst.[4b] Figure 5 characterizes the pathway for the mechanism. The $-CH_2NEt_2$ arm first dissociates from the Ru center by crossing a barrier of 20.6 kcal/mol (**TS10**), forming an intermediate **14** that is 17.4 kcal/mol higher than **6**, due to loss of coordination interaction of the ligand. The arm dissociation makes a vacant site available for coordination of the carbonate **3** to **14**. The ligand exchange to give the intermediate **15** is unfavorable; **15** is 28.5 kcal/mol higher than **6** + **3**. After carbonyl insertion into the Ru−H bond via transition state **TS11**, the alkoxide complex **16** is formed. Subsequently, the $-CH_2NEt_2$ arm closes to form the complex **17** after passing transition state **TS12**. Finally, deprotonation of the $-CH_2P^tBu_2$ arm ligand to the adjacent methoxy group affords methyl formate and methanol via transition state **TS13**. The free energy of the highest barrier (**TS13**) along the pathway, relative to **1cat** + H_2 + **3**, is 30.9 kcal/mol (**TS13**), which is 2.4 kcal/mol greater than that of **TS5** (28.5 kcal/mol relative to the same reference, the highest transition state along our predicted favorable pathway), implying that this pathway is less favorable. Note that our previous study also shows that this pathway is less favorable than the double-hydrogen-transfer pathway.[17]

The hydrogenation pathway via the $-CH_2NEt_2$ arm opening includes two separate steps: hydrogen activation (from **1cat** + H_2 → **TS1** → **6** in Figure 1) and the process described by Figure 5. As an alternative to the mechanim, we considered another possible pathway detailed in SI4 in the Supporting Information. In this pathway, the carbonate **3** first coordinates to **1cat**, and the $-CH_2NEt_2$ arm then opens to have an active site for hydrogen activation. After hydrogen activation, the reaction reaches **1cat** + **5** + MeOH via hydrogen transfer. Because the dihydrogen coordination complex (**$CodH_2$** in Figure 5) with a relative energy of 34.5 kcal/mol is already substantially higher than the highest stationary points in either Figure 1 (**TS6**, 30.8 kcal/mol) or Figure 5 (**TS13**, 30.9 kcal/mol), we exclude the possibility without characterizing all stationary points involved in this pathway. The high relative energy of **$CodH_2$** can be attributed to the loss of coordination interaction due to the $-CH_2NEt_2$ arm opening and the unfavorable dihydrogen coordination.

As an alternative to the pathway via the $-CH_2NEt_2$ arm opening, we considered the possibility of opening the $-CH_2P^tBu_2$ arm in the complex **6**. The transition state and dissociation product are 43.7 and 39.7 kcal/mol higher than the complex **6**, which are 23.1 and 22.3 kcal/mol higher than **TS10** and **14** involved in the $-CH_2NEt_2$ arm disccoation, respectively, in agreement with the general trend that phosphorus coordination is stronger than nitrogen coordination. Thus, dissociation of $-CH_2P^tBu_2$ cannot take place.

For the scenario without opening the $-CH_2NEt_2$ arm, insertion of the C═O bond of **3** into the Ru−H bond of **6** requires crossing the transition state illustrated by **$TS_{6\to9}$**. However, the geometric optimizations for **$TS_{6\to9}$** repeatedly converged to **TS2**, directly to complex **9**, or to separate complex **6** and **3** or, alternatively, drove the $-CH_2NEt_2$ arm to open (leading to no converged structures). The details for the optimization processes are given in SI6 in the Supporting Information. While we cannot absolutely exclude the existence of **$TS_{6\to9}$**, we analyzed that **$TS_{6\to9}$** would be high even if it could be located. Generally, for insertion of a double bond (e.g., alkene C═C bond) into the transition metal (TM)−H bond, the TM center needs a vacant site for coordination of the unsaturated substrates to catalysts,[38] but the Ru center in **6** is saturated and **3** cannot coordinate to the Ru center. This was implied by the observation that the optimization for **$TS_{6\to9}$** drove the $-CH_2NEt_2$ arm to open, which allows **3** to

dx.doi.org/10.1021/ic300175b | Inorg. Chem. 2012, 51, 5716−5727

coordinate to the Ru center. Indeed, when the $-CH_2NEt_2$ arm is open, as shown in Figure 5, the coordination complex **15** and the transition state (**TS11**) could be located. On the other hand, insertion of the C═O bond of **3** into the Ru−H bond of **6** can be viewed as the reverse of a β-hydrogen-elimination process from **9** to **6** + **3**. It has been well documented that the availability of a vacant site on the TM center is a prerequisite for β-hydrogen elimination. Because **9** is an 18e complex, **9** cannot revert to **6** + **3** via β-hydrogen elimination, implying that there could be no transition state between **9** and **6** + **3**. In addition, the assumed $\mathbf{TS}_{6\rightarrow 9}$ is geometrically similar to **TS6** in Figure 1 except for the formed C−H bond in **TS6**. When $\mathbf{TS}_{6\rightarrow 9}$ is compared with **TS6**, **TS6** has the formed C−H bond, while the C−H bond in $\mathbf{TS}_{6\rightarrow 9}$ has not been formed. It could be reasonable to assume that $\mathbf{TS}_{6\rightarrow 9}$ is at least higher than **TS6**. On the basis of the above analyses, we propose that the direct formation of **9** from **6** is unlikely.

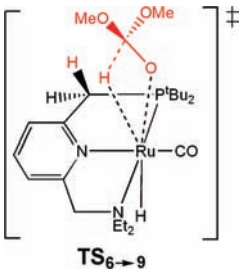

$\mathbf{TS}_{6\rightarrow 9}$

In addition to the **1cat**-mediated decomposition of hemiacetal **8**, the other two possible pathways without involving **1cat** were considered. The transition state **TS14** (Figure 6) illustrates a mechanism to form methyl formate and methanol via intermolecular proton exchange between two hemiacetal intermediates. The transition state **TS15** describes the methanol-mediated mechanism, where methanol acts as a proton-transfer bridge to facilitate intramolecular hydrogen transfer from the OH group to the OMe group. The decomposition barrier by passing **TS14**, 25.1 kcal/mol relative to two separate species (**8** + **8**), and that via **TS15**, 27.2 kcal/mol measured from **8** + methanol, are 7.9 and 10.0 kcal/mol higher than the highest barrier (**TS5**, 17.2 kcal/mol relative to the hemiacetal **8** and **1cat**) in the pathway involving the catalyst **1cat**. Therefore, the two pathways for decomposition of hemiacetal **8** are kinetically less favorable than the **1cat**-catalyzed decomposition.

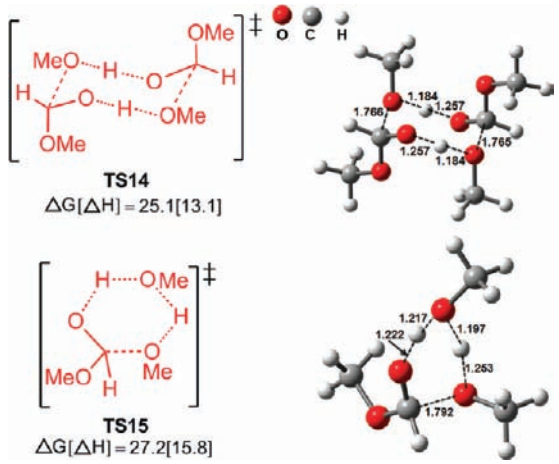

Figure 6. Optimized geometries of the transition states **TS14** and **TS15**, along with the key bond lengths in angstroms. The barriers in kilocalories per mole are relative to the separate reactants. Trivial hydrogen atoms are omitted for clarity.

3.2. Transformation of Methyl Formate 5 to Formaldehyde and Methanol (Stage II). Stage I transforms dimethyl carbonate **3** into methanol and methyl formate **5**. Stage II further transforms methyl formate **5** to formaldehyde and methanol. As shown in Figure 7, this stage follows a mechanism similar to that of stage I (see Figure 1). The hydrogen activation step is the same as that in stage I. The double hydrogen transfer takes place sequentially by passing through **TS16** and **TS17**, delivering the hemiacetal intermediate **19**. Relative to **6** + **5**, the free-energy barriers for the stepwise transfers are 18.7 (**TS16**) and 20.9 kcal/mol (**TS17**), respectively, which are lower than the corresponding values for their counterparts in stage I, being 26.0 (**TS2**) and 30.0 kcal/mol (**TS3**) relative to **6** + **3**, respectively (Figure 1B). Similar to stage I, hydrogen transfer is also endergonic by 5.0 kcal/mol measured from **6** + **5**, but the value is less than 13.5 kcal/mol in stage I. Thus, hydrogenation of methyl formate **5** is both kinetically and thermodynamically more favorable than hydrogenation of carbonate **3**. This is reasonable because the carbonyl group in methyl formate resonates with one methoxy group rather than two in carbonate, which results in relatively stronger electrophilicity of the carbonyl group in the former than in the latter. In addition, the catalyst has less steric effect with the methyl formate **5** than the dimethyl carbonate **3**, which can be observed by comparing the structures **TS16** and **TS17** (Figure 8) with their counterparts (**TS2** and **TS3** in Figure 2). Decomposition of the hemiacetal intermediate **19**, giving a second methanol and formaldehyde, proceeds along the pathway **1cat** + **19** → **TS18** → **20** → **TS19** → **21** + CH_2O. Relative to **1cat** + **19**, the free energies of **TS18**, **20**, **TS19**, and **21** + CH_2O are 17.6, 3.1, 20.1, 11.3, and 1.4 kcal/mol, respectively, which are compared with the corresponding values of 15.5, 0.4, 17.2, −0.1, and −9.7 kcal/mol for the **1cat**-mediated decomposition of hemiacatel **8**. Therefore, decomposition of **19** is kinetically and thermodynamically more favorable than decomposition of **8**. Overall, stage II is kinetically more favorable but thermodynamically less favorable than stage I; the highest barrier (**TS19**) for the former, 25.1 kcal/mol relative to **6** + **5**, is lower than the corresponding value of 30.7 kcal/mol (**TS5**) relative to **6** + **3** for the latter, and the former is thermodynamically 2.6 kcal/mol less favorable than the latter. The direct formation of **20** from **18** via the transition state **TS20** is similar to the step **7** → **TS6** → **9** in stage I. The transition state **TS20** is 7.0 and 5.3 kcal/mol higher than **TS17** and **TS18**, respectively, further implying that such a pathway is less favorable.

Our computations indicate that stages I and II take place separately, whereas the experimentalists postulated that the two stages could be coupled via **C** → **D** (Scheme 3A).[8] The possibility was considered. Agreeing with their reasoning, we hypothesized that, if **C** could activate hydrogen to give **D**, the $-CH_2NEt_2$ arm must open and rearrange the axial hydrogen of the Ru center to the equatorial position, which creates a site for hydrogen activation. The optimized structure of the transition state **TS21** for such hydrogen activation is shown in Figure 9. The barrier (58.5 kcal/mol relative to **1cat** + **5** + H_2) is too high. On the other hand, the intermediate **C** (i.e., complex **10** in Figure 1) is unstable because of the favorable entropic

dx.doi.org/10.1021/ic300175b | Inorg. Chem. 2012, 51, 5716−5727

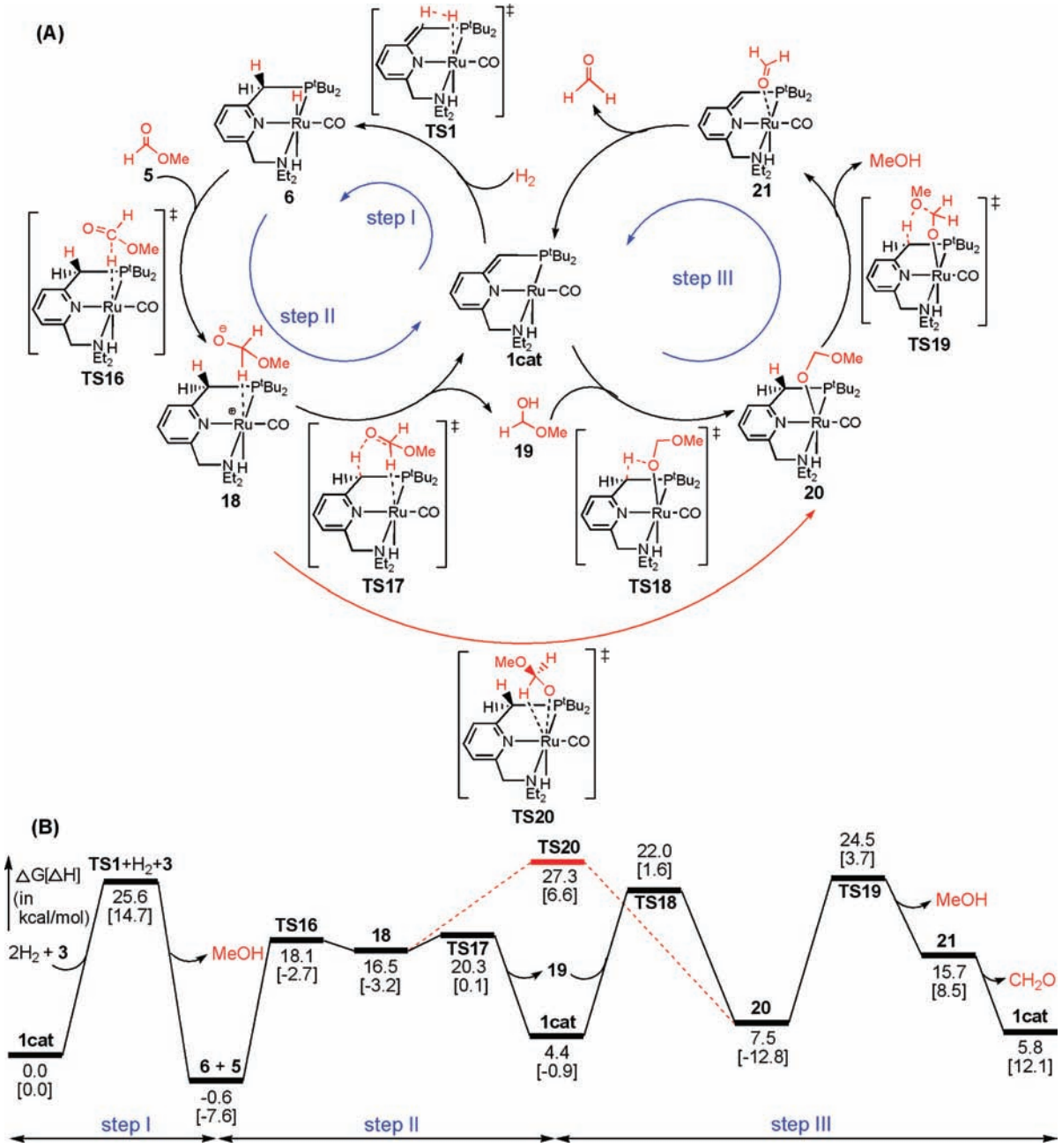

Figure 7. (A) Catalytic mechanism for hydrogenation of methyl formate **5** to formaldehyde and methanol and (B) free-energy profile corresponding to part A.

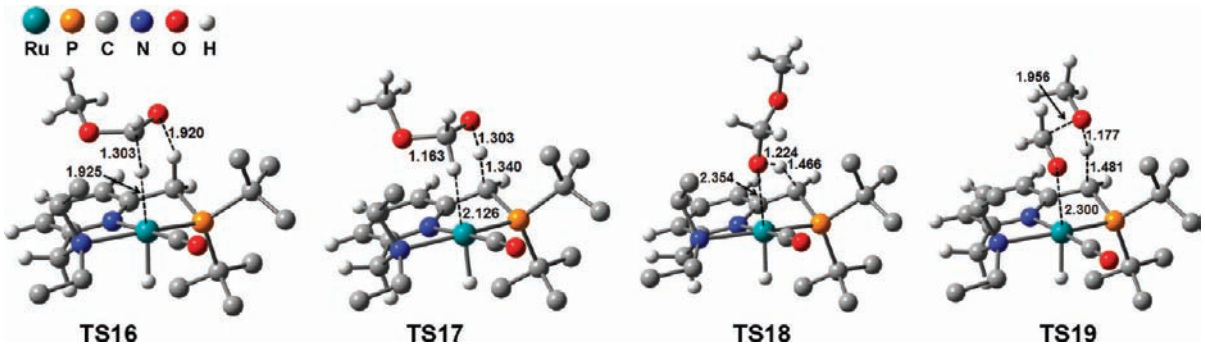

Figure 8. Optimized geometries of the key stationary points labeled in Figure 7, along with the key bond lengths in angstroms. Trivial hydrogen atoms are omitted for clarity. Other optimized geometries are given in SI7 in the Supporting Information.

dx.doi.org/10.1021/ic300175b | *Inorg. Chem.* 2012, 51, 5716–5727

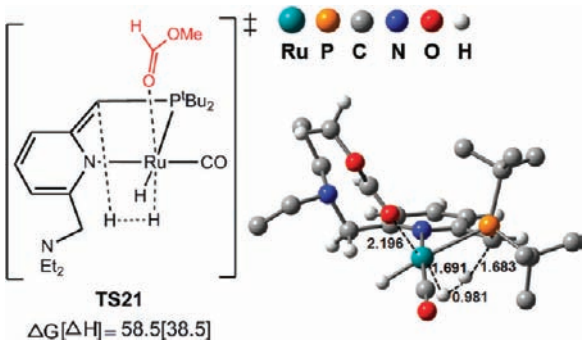

Figure 9. Optimized geometry of the transition state **TS21**, along with the key bond lengths in angstroms. The barriers in kilocalories per mole are relative to the separate reactants **1cat** + **5** + H_2. Trivial hydrogen atoms are omitted for clarity.

driving force for the release of **5**. Therefore, the possibility via the step of **C** → **D** could be excluded.

3.3. Hydrogenation of Formaldehyde to Methanol (Stage III). Formaldehyde formed in stage II can undergo hydrogenation to deliver a third methanol molecule. The pathway for hydrogenation of formaldehyde is shown in Figure 10, and the optimized structures of some key stationary points are displayed in Figure 11. Hydrogenation takes place via two steps: hydrogen activation and hydrogen transfer. The hydrogen activation is the same as that in stages I and II.

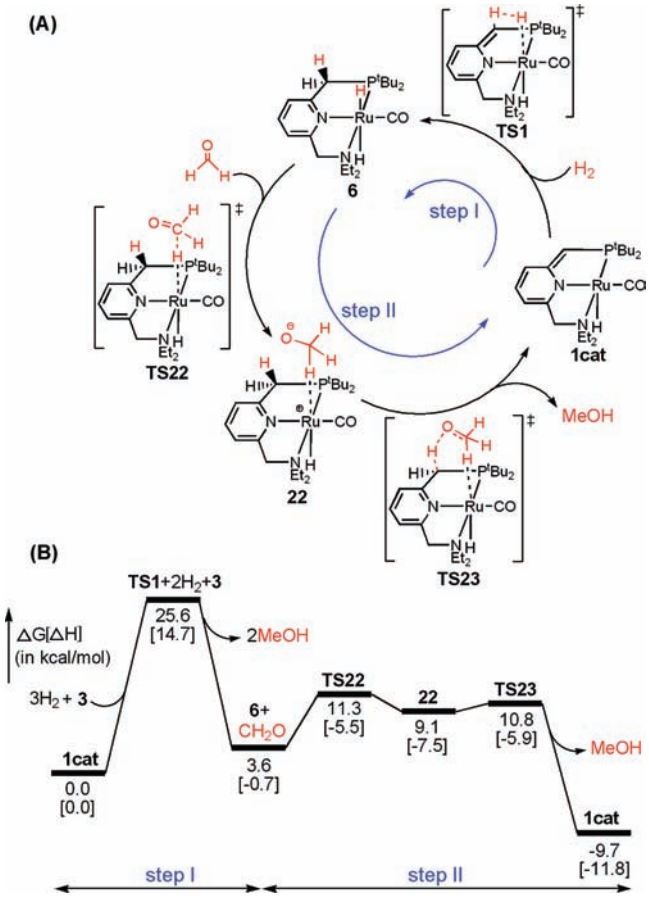

Figure 10. (A) Catalytic mechanism for hydrogenation of formaldehyde to methanol and (B) free-energy profile corresponding to part A.

The hydrogen-transfer step occurs sequentially along the pathway **6** → **TS22** → **22** → **TS23** → **1cat** + MeOH. The barriers for the two hydrogen-transfer steps via **TS22** and **TS23**, 7.7 and 7.2 kcal/mol relative to **6** + CH_2O,[39] are smaller than those [26.0 (**TS2**) and 30.0 kcal/mol (**TS3**) relative to **6** + **3**] in stage I and those [18.7 (**TS16**) and 20.9 kcal/mol (**TS17**) relative to **6** + **5**] in stage II. In contrast to the endergonic hydrogenation of dimethyl carbonate **3** and methyl formate **5**, the hydrogenation of CH_2O is exergonic by 9.7 kcal/mol. When the three hydrogenation steps in the three stages are compared, hydrogenation of CH_2O is most favorable because the electrophilicity of the carbonyl group of CH_2O is strongest and the steric repulsion between CH_2O and the catalyst **1cat** is smallest. Stages I and II are endergonic by 1.6 and 5.8 kcal/mol, respectively. Stage III is exergonic, and the complete catalytic transformation (**3** + $3H_2$ → 3MeOH) is exergonic by 9.7 kcal/mol, which is the thermodynamic driving force for stages I and II and thus for the complete transformation.

The discussion above is based on the energies computed under the conditions of 298.15 K and 1 atm, but the experiments were run under the condition of 418.15 K and 60 atm. We recalculated the energies under experimental conditions and found that, in spite of the numerical differences, the mechanisms drawn above remain true. The detailed energetic results under experimental conditions are given in SI8 in the Supporting Information.

To ascertain the mechanism drawn from the M06 (SMD)/BSII/TPSSTPSS/BSI computations, we employed M06 and ωB97X-D DFT functionals and larger basis sets to recalculate the high-energy stationary points on the basis of M06 (SMD)/BSII//TPSSTPSS/BSI energy profiles (see the Computational Details section for details). Compared in Table 1, differences can be observed in terms of the relative free-energy values among the three levels of calculations, but the mechanism sketched by Scheme 3B remains valid. (a) The pathways involving hemiacetal intermediates (i.e., **8** in stage I and **19** in stage II) are more favorable than the direct pathways at the three levels. In stage I, the pathway **7** → **TS6** → **9** is less favorable than **7** → **TS3** → **1cat** + **8** → **TS4** → **9** (**TS6** is consistently higher than both **TS3** and **TS4**), and in stage II, the **18** → **TS20** → **20** pathway is also less favorable than **18** → **TS17** → **1cat** + **19** → **TS18** → **20** (**TS20** is consistently higher than both **TS17** and **TS18**). (b) The pathway via carbonyl insertion into the Ru−H bond (Figure 5) is less favorable than the pathway (Figure 1) via double hydrogen transfer. Although the relative stabilities of **TS11** and **TS13** in the former and those of **TS3**−**TS5** in the latter may differ at the three levels, it is certain that the higher one of **TS11** and **TS13** is always higher than the highest one of **TS3**−**TS5**. (c) Methanol-aided hydrogen activation via **TS7** is more favorable than direct activation via **TS1**. (d) The intermediate **5** should be released from stage I because hydrogen activation by **C** to give **D** in Scheme 3B has a high barrier (**TS21**), 58.5, 54.5, and 56.5 kcal/mol at the three levels, respectively. (e) The mechanism proposed by Yang can be excluded in the current system because dissociation of the MeO^- group from **12** to give **13** + MeO^- is 58.7, 57.2, and 58.2 kcal/mol higher than **1cat** and methanol at the three levels, respectively.

4. CONCLUSIONS

In summary, we have carried out DFT computations to investigate the catalytic mechanism for the transformation dimethyl carbonate **3** + $3H_2$ → 3MeOH mediated by the pincer

dx.doi.org/10.1021/ic300175b | Inorg. Chem. 2012, 51, 5716−5727

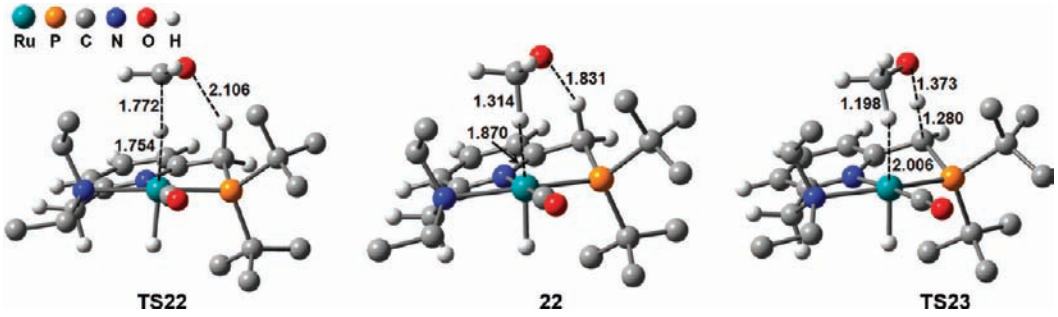

Figure 11. Optimized geometries of the key stationary points labeled in Figure 10, along with the key bond lengths in angstroms. Trivial hydrogen atoms are omitted for clarity.

Table 1. Comparisons of the Relative Free Energies (in kcal/mol) of Critical Stationary Points at Three Computational Levels (Enthalpies in kcal/mol Are Given in Brackets)

	M06/BSII//TPSSTPSS/BSI	M06/BSIV//M06/BSIII	ωB97X-D/BSIV//ωB97X-D/BSIII
TS1[a]	25.6 [14.7]	25.1 [15.0]	24.8 [14.5]
TS3[b]	27.8 [3.9]	27.4 [2.2]	21.5 [−2.7]
TS4[b]	26.8 [3.2]	26.6 [1.5]	21.1 [−4.2]
TS5[b]	28.5 [4.8]	23.5 [−0.6]	19.6 [−4.6]
TS6[b]	30.8 [7.1]	29.2 [4.5]	24.0 [−0.9]
TS7[c]	26.9 [4.7]	24.9 [2.9]	21.5 [−0.6]
13 + MeO[−d]	58.7 [57.5]	57.2 [57.1]	58.2 [55.9]
TS11[b]	30.2 [9.0]	28.0 [5.5]	23.5 [1.7]
TS13[b]	30.9 [7.3]	26.2 [2.8]	21.7 [−1.6]
TS17 + MeOH[e]	20.3[0.1]	18.9 [−1.0]	12.8 [−6.5]
TS18 + MeOH[e]	22.0 [1.6]	19.8 [0.2]	15.1 [−5.5]
TS19 + MeOH[e]	24.5 [3.7]	22.8 [2.4]	18.2 [−2.7]
TS20 + MeOH[e]	27.3 [6.6]	21.9 [3.6]	19.7 [−0.6]
TS21[f]	58.5 [38.5]	54.5 [32.4]	56.5 [33.5]

[a]Relative to **1cat** + H_2. [b]Relative to **1cat** + H_2 + **3**. [c]Relative to **1cat** + methanol + H_2. [d]Relative to **1cat** + methanol. [e]Relative to **1cat** + $2H_2$ + **3**. [f]Relative to **1cat** + H_2 + **5**.

Ru^{II}PNN catalyst. The energetic results show that, among various possible pathways leading to the products, the following pathway is most favorable. The catalytic transformation includes three sequential stages persistently involving the catalyst: (stage I) dimethyl carbonate **3** + H_2 → methyl formate **5** + MeOH; (stage II) methyl formate **5** + H_2 → formaldehyde + MeOH; (stage III) formaldehyde + H_2 → methanol. Stages I and II proceed through three steps including hydrogen activation by the catalyst, stepwise double hydrogen transfer to dimethyl carbonate (stage I) or methyl fomate (stage II), giving hemiacetal intermediates, and the subsequent decomposition of hemiacetal intermediates to afford methyl formate + MeOH or formaldehyde + MeOH. Stage III is a conventional hydrogenation process. The methanol product can further facilitate the **1cat**-promoted hydrogen activation step in the three stages. For decomposition of the hemiacetal intermediates, the catalyst breaks the O−H bond, leading to an alkoxide complex, which then undergoes deprotonation of the benzylic arm ligand to the adjacent methoxy group, leading to methanol. Other possible pathways were examined and found to be less favorable than that described above. Stages I and II are thermodynamically uphill by 1.6 and 5.8 kcal/mol, respectively, but stage III is thermodynamically downhill. The overall transformation is exergonic by 9.7 kcal/mol, which is the driving force for the catalytic reaction. When the three hydrogenation steps involved in the three stages are compared, hydrogenation of dimethyl carbonate is most difficult, that in stage II is less difficult, and that of formaldehyde is easiest in terms of both kinetics and thermodynamics. The stronger electrophilicity of the carbonyl groups bonded with one methoxy group in methyl formate or without the methoxy group in formaldehyde than that with two methoxy groups in dimethyl carbonate accounts for the easier hydrogenations of the former. In addition, the less steric effects between catalyst and methyl formate or formaldehyde could be another factor for their different reactivity.

■ ASSOCIATED CONTENT

Ⓢ Supporting Information

IRC results for selected transition states (SI1), optimized geometries of stationary points labeled in Figure 4 (SI2), details for alcohol dehydrogenation in the amide synthesis from alcohols and amines (SI3), transformation via a possible pathway including the initial coordination of methyl carbonate (**3**) to **1cat**, the $-CH_2NEt_2$ arm opening, dihydrogen coordination, and hydrogen transfer (SI4), optimized geometries of stationary points labeled in Figure 5 (SI5), details for optimizing $\mathbf{TS_{6\rightarrow 9}}$, which directly leads to **9** via insertion of the C═O bond of **3** into the Ru−H bond of **6** (SI6), optimized geometries of stationary points labeled in Figure 7 but not shown in Figure 8 (SI7), free-energy profiles under the experiment conditions (T = 418.15 K; P = 60 atm) (SI8), complete information for refs 29 and 30 (SI9), and Cartesian coordinates and absolute energies for the stationary points in the text (SI10). This material is available free of charge via the Internet at http://pubs.acs.org.

■ AUTHOR INFORMATION

Corresponding Author

*E-mail: zxwang@gucas.ac.cn.

Notes

The authors declare no competing financial interest.

■ ACKNOWLEDGMENTS

This work is supported financially by the Chinese Academy of Science and the National Science Foundation of China (Grants 20973197 and 21173263).

REFERENCES

(1) de Vries, J. G.; Elsevier, C. J. *The Handbook of Homogeneous Hydrogenation*; Wiley-VCH: Weinheim, Germany, 2007.

(2) Nishimura, S. *The Handbook of Heterogeneous Catalytic Hydrogenation for Organic Synthesis*; Wiley: New Youk, 2001.

(3) For representative reviews on the hydrogenations catalyzed by TM complexes, see: (a) Clapham, S. E.; Hadzovic, A.; Morris, R. H. *Coord. Chem. Rev.* **2004**, *248*, 2201. (b) Gladiali, S.; Alberico, E. *Chem. Soc. Rev.* **2006**, *35*, 226. (c) Ikariya, T.; Murata, K.; Noyori, R. *Org. Biomol. Chem.* **2006**, *4*, 393. (d) Samec, J. S. M.; Bäckvall, J.-E.; Andersson, P. G.; Brandt, P. *Chem. Soc. Rev.* **2006**, *35*, 237. (e) Ito, M.; Ikariya, T. *Chem. Commun.* **2007**, *43*, 5134. (f) O, W. W. N.; Lough, A. J.; Morris, R. H. *Chem. Commun.* **2010**, *46*, 8240.

(4) (a) Teunissen, H. T.; Elsevier, C. J. *Chem. Commun.* **1998**, 1367. (b) Zhang, J.; Leitus, G.; Ben-David, Y.; Milstein, D. *Angew. Chem., Int. Ed.* **2006**, *45*, 1113. (c) Saudan, L. A.; Saudan, C. M.; Debieux, C.; Wyss, P. *Angew. Chem., Int. Ed.* **2007**, *46*, 7473. (d) Fogler, E.; Balaraman, E.; Ben-David, Y.; Leitus, G.; Shimon, L. J. W.; Milstein, D. *Organometallics* **2011**, *30*, 3826. (e) Zhang, J.; Balaraman, E.; Leitus, G.; Milstein, D. *Organometallics* **2011**, *30*, 5716.

(5) (a) Núñez Magro, A. A.; Eastham, G. R.; Cole-Hamilton, D. J. *Chem. Commun.* **2007**, *43*, 3154. (b) Balaraman, E.; Gnanaprakasam, B.; Shimon, L. J. W.; Milstein, D. *J. Am. Chem. Soc.* **2010**, *132*, 16756.

(6) (a) The value of 6.2 kcal/mol is the ΔG difference ($\Delta\Delta G$) of the two reactions [MeC(O)OMe + H_2 → MeCH(OH)OMe + ΔG and $Me_2C{=}O$ + H_2 → Me_2CHOH + ΔG]. (b) The value of 11.3 [2.5] kcal/mol is the ΔG [ΔH] value of the reaction MeOC(O)OMe + H_2 → MeOCH(OH)OMe. Both values were calculated at the default level used in the present study (see the Computational Details section).

(7) (a) Gormley, R. J.; Rao, V. U. S.; Soong, Y.; Micheli, E. *Appl. Catal., A* **1992**, *87*, 81. (b) Iwasa, N.; Terashita, M.; Arai, M.; Takezawa, N. *React. Kinet. Catal. Lett.* **2001**, *74*, 93.

(8) Balaraman, E.; Gunanathan, C.; Zhang, J.; Shimon, L. J. W.; Milstein, D. *Nat. Chem.* **2011**, *3*, 609.

(9) Balaraman, E.; Ben-David, Y.; Milstein, D. *Angew. Chem., Int. Ed.* **2011**, *50*, 11702.

(10) Schaeffner, B.; Schaeffner, F.; Verevkin, S. P.; Boerner, A. *Chem. Rev.* **2010**, *110*, 4554.

(11) (a) Sakakura, T.; Choi, J.-C.; Yasuda, H. *Chem. Rev.* **2007**, *107*, 2365. (b) Sakakura, T.; Kohno, K. *Chem. Commun.* **2009**, *45*, 1312.

(12) Gunanathan, C.; Milstein, D. *Acc. Chem. Res.* **2011**, *44*, 588.

(13) (a) Ben-Ari, E.; Leitus, G.; Shimon, L. J. W.; Milstein, D. *J. Am. Chem. Soc.* **2006**, *128*, 15390. (b) Kohl, S. W.; Weiner, L.; Schwartsburd, L.; Konstantinovski, L.; Shimon, L. J. W.; Ben-David, Y.; Iron, M. A.; Milstein, D. *Science* **2009**, *324*, 74. (c) Gunanathan, C.; Gnanaprakasam, B.; Iron, M. A.; Shimon, L. J. W.; Milstein, D. *J. Am. Chem. Soc.* **2010**, *132*, 14763. (d) Khaskin, E.; Iron, M. A.; Shimon, L. J. W.; Zhang, J.; Milstein, D. *J. Am. Chem. Soc.* **2010**, *132*, 8542. (e) Zeng, H. X.; Guan, Z. B. *J. Am. Chem. Soc.* **2011**, *133*, 1159.

(14) (a) Iron, M. A.; Ben-Ari, E.; Cohen, R.; Milstein, D. *Dalton Trans.* **2009**, 9433. (b) Li, J.; Shiota, Y.; Yoshizawa, K. *J. Am. Chem. Soc.* **2009**, *131*, 13584. (c) Zeng, G.; Guo, Y.; Li, S. *Inorg. Chem.* **2009**, *48*, 10257. (d) Schwartsburd, L.; Iron, M. A.; Konstantinovski, L.; Diskin-Posner, Y.; Leitus, G.; Shimon, L. J. W.; Milstein, D. *Organometallics* **2010**, *29*, 3817.

(15) (a) Yang, X. Z.; Hall, M. B. *J. Am. Chem. Soc.* **2010**, *132*, 120. (b) Chen, Y.; Fang, W.-H. *J. Phys. Chem. A* **2010**, *114*, 10334. (c) Sandhya, K. S.; Suresh, C. H. *Organometallics* **2011**, *30*, 3888. (d) Zeng, G.; Li, S. *Inorg. Chem.* **2011**, *50*, 10572. (e) Yang, X. Z. *ACS Catal.* **2011**, *1*, 849.

(16) Lu, G.; Li, H.; Zhao, L.; Huang, F.; Schleyer, P. V.; Wang, Z.-X. *Chem.—Eur. J.* **2011**, *17*, 2038.

(17) Li, H.; Wang, X.; Huang, F.; Lu, G.; Jiang, J.; Wang, Z.-X. *Organometallics* **2011**, *30*, 5233.

(18) Tao, J. M.; Perdew, J. P.; Staroverov, V. N.; Scuseria, G. E. *Phys. Rev. Lett.* **2003**, *91*, 146401.

(19) Hay, P. J.; Wadt, W. R. *J. Chem. Phys.* **1985**, *82*, 299.

(20) (a) Zhao, Y.; Truhlar, D. G. *J. Chem. Phys.* **2006**, *125*, 194101. (b) Zhao, Y.; Truhlar, D. G. *Acc. Chem. Res.* **2008**, *41*, 157.

(21) Marenich, A. V.; Cramer, C. J.; Truhlar, D. G. *J. Phys. Chem. B* **2009**, *113*, 6378.

(22) Andrae, D.; Häussermann, U.; Dolg, M.; Stoll, H.; Preuss, H. *Theor. Chim. Acta* **1990**, *77*, 123.

(23) (a) Hermans, J.; Wang, L. *J. Am. Chem. Soc.* **1997**, *119*, 2707. (b) Strajbl, M.; Sham, Y. Y.; Villa, J.; Chu, Z. T.; Warshel, A. *J. Phys. Chem. B* **2000**, *104*, 4578. (c) Yu, Z.-X.; Houk, K. N. *J. Am. Chem. Soc.* **2003**, *125*, 13825.

(24) Liang, Y.; Liu, S.; Xia, Y. Z.; Li, Y. H.; Yu, Z.-X. *Chem.—Eur. J.* **2008**, *14*, 4361.

(25) (a) Ben-Naim, A.; Marcus, Y. *J. Chem. Phys.* **1984**, *81*, 2016. (b) Tissandier, M. D.; Cowen, K. A.; Feng, W. Y.; Gundlach, E.; Cohen, M. H.; Earhart, A. D.; Coe, J. V.; Tuttle, T. R. *J. Phys. Chem. A* **1998**, *102*, 7787. (c) Kelly, C. P.; Cramer, C. J.; Truhlar, D. G. *J. Phys. Chem. B* **2006**, *110*, 16066. (d) Lopes, P. E. M.; Roux, B.; MacKerell, A. D. *Theor. Chem. Acc.* **2009**, *124*, 11.

(26) Martin, R. L.; Hay, P. J.; Pratt, L. R. *J. Phys. Chem. A* **1998**, *102*, 3565.

(27) Chai, J.-D.; Head-Gordon, M. *Phys. Chem. Chem. Phys.* **2008**, *10*, 6615.

(28) The Role of Databases in Support of Computational Chemistry Calculations: Feller, D. *J. Comput. Chem.* **1996**, *17*, 1571. Basis Set Exchange: A Community Databases for Computational Sciences: Schuchardt, K. L.; Didier, B. T.; Elsethagen, T.; Sun, L.; Gurumoorthi, V.; Chase, J.; Li, J.; Windus, T. L. J. *Chem. Inf. Model.* **2007**, *47*, 1045.

(29) Frisch, M. J. *Gaussian 03*, revision E.01; Gaussian, Inc.: Wallingford, CT, 2004.

(30) Frisch, M. J. *Gaussian 09*; revision A.01; Gaussian, Inc.: Wallingford, CT, 2009.

(31) (a) Yamakawa, M.; Ito, H.; Noyori, R. *J. Am. Chem. Soc.* **2000**, *122*, 1466. (b) Abdur-Rashid, K.; Clapham, S. E.; Hadzovic, A.; Harvey, J. N.; Lough, A. J.; Morris, R. H. *J. Am. Chem. Soc.* **2002**, *124*, 15104.

(32) (a) Zhao, L.; Li, H.; Lu, G.; Wang, Z.-X. *Dalton Trans.* **2010**, *39*, 4038. (b) Li, H.; Zhao, L.; Lu, G.; Huang, F.; Wang, Z.-X. *Dalton Trans.* **2010**, *39*, 5519. (c) Zhao, L.; Li, H.; Lu, G.; Huang, F.; Zhang, C.; Wang, Z.-X. *Dalton Trans.* **2011**, *40*, 1929.

(33) (a) Ikariya, T.; Blacker, A. J. *Acc. Chem. Res.* **2007**, *40*, 1300. (b) Morris, R. H. *Chem. Soc. Rev.* **2009**, *38*, 2282. (c) Sui-Seng, C.; Haque, F. N.; Hadzovic, A.; Pütz, A.-M.; Reuss, V.; Meyer, N.; Lough, A. J.; Iuliis, M. Z.-D.; Morris, R. H. *Inorg. Chem.* **2009**, *48*, 735.

(34) (a) Casey, C. P.; Johnson, J. B.; Singer, S. W.; Cui, Q. *J. Am. Chem. Soc.* **2005**, *127*, 3100. (b) Hadzovic, A.; Song, D.; MacLaughlin, C. M.; Morris, R. H. *Organometallics* **2007**, *26*, 5987.

(35) For selected references of H_2O-assisted hydrogen release, see: (a) Wu, X. F.; Liu, J. K.; Di Tommaso, D.; Iggo, J. A.; Catlow, C. R. A.; Bacsa, J.; Xiao, J. L. *Chem.—Eur. J.* **2008**, *14*, 7699. (b) Friedrich, A.; Drees, M.; auf der Günne, J. S.; Schneider, S. *J. Am. Chem. Soc.* **2009**, *131*, 17552.

(36) Yang, X. *Inorg. Chem.* **2011**, *50*, 12836.

(37) For recent reviews, see: (a) Lein, M. *Coord. Chem. Rev.* **2009**, *253*, 635. (b) Brookhart, M.; Green, M. L. H.; Parkin, G. *Proc. Natl. Acad. Sci. U.S.A.* **2007**, *104*, 6908.

(38) Crabtree, R. H. *The Organometallic Chemistry of the Transition Metals*; John Wiley & Sons, Inc.: Hoboken, NJ, 2005.

(39) In terms of enthalpy, **TS22** is lower than **6** and CH_2O, it seems unreasonable to optimize **TS22**, but note that there is a complex between **6** and CH_2O before **TS22**, which is 0.3 kcal/mol lower than **TS22** in terms of the electronic energy. Thus, **TS22** could be optimized.

dx.doi.org/10.1021/ic300175b | *Inorg. Chem.* 2012, 51, 5716−5727